On magnetoconductivity of metallic manganite phases and heterostructures

M. Dzero *,[1], L. P. Gor'kov[1,2], and V. Z. Kresin[3]
[1] *National High Magnetic Field Laboratory, Florida State University, Tallahassee, FL 32310*
[2] *L.D. Landau Institute for Theoretical Physics, Russian Academy of Sciences, 117334 Moscow, Russia and*
[3] *Lawrence Berkeley Laboratory, University of California, Berkeley, CA 94720*

We use the double exchange (DE) model via degenerate orbitals and tight-binding approximation to study the magnetoconductivity of a canted A-phase of pseudo-cubic manganites. It is argued that the model is applicable in a broad concentration range for manganites $A_{1-x}B_xMnO_3$ with the tolerance factor, t, close to one. As for the substitutional disorder, scattering on random Jahn-Teller distortions of MnO_6 octahedra is chosen. We emphasize an intimate correlation between the carrier concentration and resistivity value of metallic manganites. Magnetoresistance as a function of magnetization is calculated for a canted A-phase for both in-plane and out-of-plane current directions. A contact between two manganite phases is considered and structure of the transition region near the contact is discussed. Numerical calculations show charge re-distribution near the contact and a large screening length of the order of five inter-atomic distances. We employed our results to interpret data obtained in recent experiments on $La_{0.4}Sr_{0.6}MnO_3/La_{0.55}Sr_{0.45}MnO_3$ superlattices. We also briefly discuss the relative importance of the cooperative Jahn-Teller distortions, double exchange mechanism and super-exchange interactions for the formation of the A-phase at increasing Sr concentrations $x > 0.45$ in $La_{1-x}Sr_xMnO_3$ to suggest that the Jahn-Teller contraction of octahedra, $c/a < 1$, plays a prevailing role.

PACS numbers: 75.30.-m, 75.30.Vn, 75.50.Ee, 75.70.-i

I. INTRODUCTION

Pseudo-cubic manganites are remarkable for their rich phase diagram although properties of various phases have not been studied equally well. For example, the mechanisms of the "charge ordering" phenomenon (CO-phase) or of the metallic anti-ferromagnetic phase (A-phase), which usually appear near $x \simeq 0.5$, to a large extent remain to be poorly understood. It is also surprising that the potential of metallic manganites as the basic elements for various hetero-structures in development of alternate devices is practically unexplored. Meanwhile the diversity of their phases depending on temperature and doping concentration poses interesting questions regarding phenomena that may take place at the interface of the contacts between them. Further understanding of magneto-transport properties of these materials also remains of prime importance because of several reasons. One of them is the colossal magneto-resistance effect, observed in these compounds at room temperatures. At the same time there is an increased general interest in the artificial engineering of nano-structure materials with novel physical properties, such as the giant magneto-resistance (GMR) effect (see[1] for a review). The discovery of the GMR effect has generated a lot of investigations focused on understanding the physical mechanism of this phenomena and that is why use of artificial hetero-structures composed of manganites suggests an interesting direction of research. Indeed, the A-phase with its weakly coupled ferromagnetic planes is a natural spin-valve system itself [2]. Recent experimental results for large magneto-resistance on the domain walls in strained ferromagnetic manganite films provide another interesting example of such properties that may become important for various applications[3]. Last but not least is a richness of magnetic and transport properties of manganites. Concentration dependence and even overall topology pattern of the phase diagram varies from material to material in these compounds with general formula $A_{1-x}B_xMnO_3$ (A=La, Pr, Nd; B=Sr, Ca)[4]. In what follows we concentrate our attention mainly on $La_{1-x}Sr_xMnO_3$ (LSMO) compounds because there are no complications due to "charge ordering". Instead their phase diagram is remarkable for the metallic ferromagnetic and metallic anti-ferromagnetic phases inside the concentration ranges ($0.3 \leq x \leq 0.5$) and ($0.5 \leq x \leq 0.7$) correspondingly[4]. In addition, the LSMO compounds allow the use of band description for broad concentration range.

Usually among the main difficulties in trying to describe the properties of magnetic hetero-structures on the theory part lies the fact that a contact area between the two materials with different magnetic ordering corresponds to an abrupt change in the underlying ground states: microscopic effects at the boundaries, values of transmission coefficients of carriers, change in the exchange mechanisms between the core spins *etc.*, all of them taking place at the contact on the atomic scale. We are motivated by the idea that the boundary between two manganite phases

* Also at: Physics Department, Florida State University. Electronic address: dzero@magnet.fsu.edu

with rather close doping levels may present a better ground for the understanding of interface phenomena. It is worth mentioning, that attempts to fabricate and investigate the characteristics of manganite hetero-structures have already been made[5,6].

In this paper we pursue a study of an electronic spectrum, mechanisms of conductivity and magneto-conductivity of both the ferromagnetic and anti-ferromagnetic (A-phase) phases. In particular, we address the phenomena that may appear at the interface of their contact. We use our results as an attempt to rationalize some experimental observations[5] performed on films and hetero-structures made of manganites having these two phases as ground states.

Manganites are thought to belong to the group of the materials with strongly correlated electrons. As it was mentioned above, their phase diagram consists of numerous phases, with a crossover from one phase to another upon change in temperature T, doping concentration x or composition, $A_{1-x}B_xMnO_3$, (see, for example[7,8,9] and references therein). The parent $LaMnO_3$ compound has the anti-ferromagnetic insulating state (A$'$) at low temperatures. Upon Sr substitution with La above $x > x_{cr} = 0.16 \div 0.17$, it undergoes a transition to a ferromagnetic (FM) metallic state. With further increase in doping ($x \geq 0.5$), as it was mentioned above, there is a transition from a ferromagnetic metallic to another anti-ferromagnetic metallic state (A-phase). The latter is defined as the phase, in which the core (t_{2g}) spins are aligned ferromagnetically in the planes (for example, ab-plane) and anti-ferromagnetically along the axis perpendicular to the planes (c-axis). In the ferromagnetic phase electrons are fully polarized ("half-metallic" state). The "half-metallic" state is also realized inside the ab-planes of the A-phase. Below we restrict our consideration to low temperatures.

Despite of the mutual consent on the prevailing role of the double exchange (DE) mechanism[10] as the basic mechanism responsible for ferromagnetism in manganites, there are several theories describing their low-temperature properties from different perspectives (for a recent review, see[11]). For our purposes it is worth mentioning right here that for the concentration range $0.3 \leq x \leq 0.75$, the physical properties of the LSMO compounds at least at low temperatures can be accounted for within the double exchange (DE) model generalized for the degenerate orbitals[12,13]. The scheme suggested in[12,13,14] is basically the band model utilizing however such important features of manganites as large values of Hund's coupling constant, J_H, and double degeneracy of the e_g orbitals. It was shown to be capable of some predictions regarding the evolution of the physical characteristics with change in electron concentration upon doping. At larger concentrations the super-exchange interaction between the t_{2g} core spins also plays an important role[13].

The fact that the band picture captures the main physics of manganites is not obvious. Often a generalized Hubbard model is used to account for strong electron-electron interactions[15]. However, instead of a direct Hubbard on-site $U > 0$ which hinders the double occupation on each Mn site, one may consider the local Jahn-Teller effect as another way to describe the same physics. Indeed, a single electron positioned on the degenerate e_g-orbital of the Mn site will cause a local lattice distortion, reducing the energy of a system. On the other hand two electrons on the same site do not lead to Jahn-Teller instability and the Jahn-Teller energy gain does not realize itself. Therefore in the local picture it is energetically favorable to have a single electron on a given site. We should also mention the large values of the Hund's coupling ($J_H \simeq 1$eV), which is responsible for the polarization of all electrons on the Mn site. A tendency to the Jahn-Teller effect causes strong electron-phonon interaction which is thought to be the reason for various structural transitions in manganites, affecting their electronic properties.

The Jahn-Teller instability is inherent to the *local* high-spin ($S = 2$) configuration of a manganese ion due to double degeneracy of the e_g orbitals. When such an instability realizes itself as a *cooperative* Jahn-Teller transition, it also accounts for the Coulomb interactions in a system, as it was discussed above. In addition the coherent long-range order correlations of the local distortions along the crystal lattice favor the band description for electrons. Stability of the anti-ferromagnetic (A'-phase) for the parent $LaMnO_3$ compound was indeed explained in Ref. [12] in terms of the Jahn-Teller cooperative effect incorporated into the two-band tight-binding approximation.

A primary manifestation of the Jahn-Teller effect comes about with an appearance of a proper deformation of the MnO_6 octahedron. However substitutional doping also leads to the lattice deformations. Mismatch between the sizes of different ions is expressed by the value of the tolerance factor, t:

$$t = \frac{1}{\sqrt{2}} \cdot \frac{R_B + R_O}{R_A + R_O},$$

where $R_i (i = A, B, O)$ are the ionic radii of each element in $A_{1-x}B_xMnO_3$. A process of doping results in an average change of the lattice parameters, which may be described by the average $\langle t \rangle_{av}$. When the value of $\langle t \rangle_{av}$ is close to 1, the "cubic" perovskite structure is realized as a whole. One must distinguish $\langle t \rangle_{av}$ from its "local" value: two materials may have close $\langle t \rangle_{av}$, i.e. close lattice parameters, but the local distortions or disorder may differ strongly from one site to another. Experiments show (see[7] and references there in) that two compounds with close overall $t \simeq 1$ often have very different values of residual resistivity, ρ_0. Analysis in terms of the band electrons is applicable if local disorder remains reasonably small, i.e. the mean free path of electrons is large enough. From this point of view, the considerable differences in the values of conductivity of various ferromagnetic manganites at the same doping level

should be ascribed to strong variations in the values of the local tolerance factor. With the increase in disorder the mean free path may become so short that the Anderson mobility edge would hinder metallic conductivity even in the ferromagnetic phase. Such an unifying view turns out to be rather helpful for classification of the physical properties of the whole series of doped manganites[12].

Before proceeding further another simple observation regarding the role of the Jahn-Teller instability can be made. At $x = 0$, according to[12], the A'-phase in $LaMnO_3$ is in the cooperative state with all bands filled up by electrons. The Sr doping lifts the local degeneracy of the e_g orbitals and introduces random strains in the lattice. De-localization in the electronic bands and hence gain in the kinetic energy also competes with *cooperative* Jahn-Teller effects. Therefore, it is expected that at intermediate concentrations x the A'- phase is destroyed resulting in an appearance of the ferromagnetic phase in the framework of the DE mechanism. There is no electron-hole symmetry in the two orbital model. At $x = 1$ there are no electrons in the system and, therefore, departing from the "other end" of the phase diagram, $x \to 1$, small number of carriers, $1 - x$, experience the Jahn-Teller instability and should be trapped locally at the Mn sites. With an increase in the number of electrons, local Jahn-Teller traps will merge into a coherent state which is responsible for another lattice structure with the directions of spins remaining to be arranged. Although the cooperative Jahn-Teller effect seems to be a major mechanism responsible for the diversity of the phase diagram of manganites at $x \simeq 0.5$ and higher, spin interactions must be included to finally specify the resulting ground states[11,13].

Due to the small differences in ionic radii between the La and Sr atoms ($t \simeq 1$), it seems, that the band description works best for $La_{1-x}Sr_xMnO_3$ compounds[12]. For these materials, being in the ferromagnetic metallic state, the residual resistivity can be as small as $\rho_0 \simeq 10^{-5} \div 10^{-4}$ $(\Omega \cdot cm)$[16], which is a good metallic conductivity range. Unfortunately, so far there are not so many experimental papers that deal with LSMO. Nevertheless, there are few[5,8,16,17,18] and in what follows we keep LSMO materials in mind in our approach to different phenomena.

In this paper we first study the magneto-transport properties of the manganites for a more general case of a *canted* A-phase[19]. This term means that the core t_{2g} spins of the Mn ions maintain both the FM and AFM components (e.g. spins in the A-phase can be canted by applying an external magnetic field). We first derive an expression for the energy spectrum of electrons for the canted A-phase manganites (Section II) and then proceed with the derivation of the formulas for the magneto-conductivity by generalizing the diagrammatic "cross" technique[20] for Green functions in the two-band model (Section III). Specific case of manganites makes a modification in the form of the "impurity potentials" necessary, to include a dependence on the orbital indexes. More specifically, the distortions of the Mn-O-Mn conduction network are primarily caused by random octahedral distortions. With Sr doping, the number of distorted octahedron increases so that one may expect a correlation between the number of carriers and the value of conductivity even for the high-quality samples.

Throughout this paper we use the tight binding approximation in the frame of the two-orbital DE model[12]. This model, as we already mentioned, has proved to capture the main physical properties of manganites at least in the metallic concentration range. Finally in Section IV we briefly discuss phenomena in the vicinity of the interface between the A-phase and FM-phase manganites. The details of our numerical calculations with some exact results are provided in Appendix. In the concluding Section together with a general discussion an attempt also made to apply the results to recent experiments on $La_{0.45}Sr_{0.55}MnO_3/La_{0.6}Sr_{0.4}MnO_3$ superlattices[5].

II. ENERGY SPECTRUM OF CANTED A-PHASE

We start directly with a general case of the canted A-phase magnetic structure. The band Hamiltonian has the form:

$$\widehat{H} = \sum_{\mathbf{p}} T^{\alpha\beta}(\boldsymbol{p})\ \widehat{a}^{\dagger}_{\alpha\sigma}(\boldsymbol{p})\ \widehat{a}_{\beta\sigma}(\boldsymbol{p}) + J_H \sum_{\mathbf{p},\mathbf{Q}} S(\boldsymbol{Q})\ \widehat{a}^{\dagger}_{\alpha\sigma'}(\boldsymbol{p})(\widehat{\sigma}_z)_{\sigma'\sigma''}\ \widehat{a}_{\alpha\sigma''}(\boldsymbol{p}-\boldsymbol{Q}) +$$

$$J_H \sum_{\mathbf{p},\mathbf{Q}} S(-\boldsymbol{Q})\ \widehat{a}^{\dagger}_{\alpha\sigma'}(\boldsymbol{p})(\widehat{\sigma}_z)_{\sigma'\sigma''}\ \widehat{a}_{\alpha\sigma''}(\boldsymbol{p}+\boldsymbol{Q}) + J_H M \sum_{\mathbf{p}}\ \widehat{a}^{\dagger}_{\alpha\sigma'}(\boldsymbol{p})(\widehat{\sigma}_x)_{\sigma'\sigma''}\ \widehat{a}_{\alpha\sigma''}(\boldsymbol{p}). \qquad (1)$$

Here $T^{\alpha\beta}(\boldsymbol{p})$ is an electron hopping matrix for the two-band model, J_H is the Hund's coupling constant on the Mn sites, and $S(\boldsymbol{Q})$ is the Fourier component of the AF ordering along the c direction, $S_z(i) = \langle S_z \rangle (-1)^i$. The magnetic structural vector $\boldsymbol{Q} = (0, 0, \pi/a)$ reduces Brillouin zone (a is the cubic lattice constant); M is a canted magnetic moment, so that at each site i:

$$\boldsymbol{S}(i) = (M_x, \pm\langle S_z \rangle),\ S_z^2 + M_x^2 \simeq S^2$$

(when $S_z(\boldsymbol{Q}) = 0$ we obtain the ferromagnetic phase). The orientations of M and S_z are fixed by magnetic anisotropy (easy plane) and/or by an external field. The matrix elements $T^{\alpha\beta}(\boldsymbol{p})$ in the Eq.(1) are calculated with the basis

functions of the following form[12]:

$$\psi_1 \propto z^2 + e^{i2\pi/3}x^2 + e^{-i2\pi/3}y^2, \psi_2 = \psi_1^*, \tag{2}$$

As the result the hopping matrix elements are equal to:

$$T^{\alpha\beta}(\boldsymbol{p}) = |A| \begin{pmatrix} T^{11}(\boldsymbol{p}) & T^{12}(\boldsymbol{p}) \\ T^{21}(\boldsymbol{p}) & T^{22}(\boldsymbol{p}) \end{pmatrix}, \tag{3}$$

where

$$T^{11}(\boldsymbol{p}) = T^{22}(\boldsymbol{p}) = \cos(p_x a) + \cos(p_y a) + \cos(p_z a),$$
$$T^{12}(\boldsymbol{p}) = \left(T^{21}\right)^*(\boldsymbol{p}) = \cos(p_z a) + e^{i2\pi/3}\cos(p_x a) + e^{-i2\pi/3}\cos(p_y a)$$

and $|A| \simeq 0.16$eV being a hopping amplitude[12].

From (1) we obtain the following equation of motion:

$$\left(E\delta_{\alpha\beta} - T^{\alpha\beta}(\boldsymbol{p})\right) \widehat{a}_{\beta\sigma}(\boldsymbol{p}) = J_H S(\boldsymbol{Q})(\widehat{\sigma}_z)_{\sigma,\sigma'}\widehat{a}_{\alpha\sigma'}(\boldsymbol{p}-\boldsymbol{Q}) + J_H M(\widehat{\sigma}_x)_{\sigma,\sigma'}\widehat{a}_{\alpha\sigma'}(\boldsymbol{p}) \tag{4}$$

and similar equation for $\boldsymbol{p} \to \boldsymbol{p}+\boldsymbol{Q}$. Thus, the secular equation, is now an 8×8 determinant from which one must calculate the eigenvectors and eigenvalues. Let us remind that the double exchange (DE) mechanism for the manganites[10] exploits the large value of the Hund interaction, $J_H \approx 1 \div 2$ eV, so that $J_H/|A| \gg 1$. Using this approximation, we solve Eq. (4) up to the terms of the order of $|A|^2/J_H$. The electrons can occupy only four lowest bands:

$$\begin{aligned} E_{1,2}(\boldsymbol{p}; M/S) &= -J_H S - |A|\cdot[c_x + c_y + (M/S)c_z \pm R_{12}(\boldsymbol{p}; M/S)], \\ E_{3,4}(\boldsymbol{p}; M/S) &= -J_H S - |A|\cdot[c_x + c_y - (M/S)c_z \pm R_{34}(\boldsymbol{p}; M/S)], \end{aligned} \tag{5}$$

where for brevity we introduced the notations $c_i \equiv \cos(p_i a), i = x, y, z$ and

$$R_{12}(\boldsymbol{p}; M/S) = \sqrt{c_x^2 + c_y^2 + (M/S)^2 c_z^2 - (M/S)c_z(c_x + c_y) - c_x c_y},\ R_{34}(\boldsymbol{p}; M/S) = R_{12}(\boldsymbol{p}; -M/S).$$

Performing the canonical transformation in accordance with the eigenvalues of Eqs. (5), it is straightforward to express operators $\widehat{a}^\dagger_{\alpha\sigma}(\boldsymbol{p})$ and $\widehat{a}_{\alpha\sigma}(\boldsymbol{p})$ in Eq. (1) in terms of the new eigenfunctions. Quite generally, the transformation has the form:

$$\widehat{a}_{\alpha\sigma}(\boldsymbol{p}) = \sum_{l=1}^{8} K^{(l)}_{\alpha\sigma}(\boldsymbol{p}) \cdot \widehat{\zeta}_l(\boldsymbol{p}), \tag{6}$$

where $\widehat{\zeta}^\dagger_l(\boldsymbol{p}), \widehat{\zeta}_l(\boldsymbol{p})$ are creation and annihilation operators for the true energy branches (5), $\sigma \equiv (\uparrow\downarrow)$. Below we write down explicitly the expressions for $K^{(l)}_{\alpha\sigma}$ for the four lowest bands:

$$K^{(1)}_{1\sigma}(\boldsymbol{p}) = K^{(2)}_{1\sigma}(\boldsymbol{p}) = \frac{1}{2}(1+M/S)^{1/2}\left(\frac{\Sigma_{12}(\boldsymbol{p})}{2R_{12}(\boldsymbol{p})}\right)^{1/2},\ K^{(1)}_{2\sigma}(\boldsymbol{p}) = -K^{(2)}_{2\sigma}(\boldsymbol{p}) = \frac{1}{2}(1+M/S)^{1/2}\left(\frac{\Sigma^*_{12}(\boldsymbol{p})}{2R_{12}(\boldsymbol{p})}\right)^{1/2},$$
$$K^{(3,4)}_{1\uparrow}(\boldsymbol{p}) = -K^{(3,4)}_{1\downarrow}(\boldsymbol{p}) = \frac{1}{2}(1-M/S)^{1/2}\left(\frac{\Sigma_{34}(\boldsymbol{p})}{2R_{34}(\boldsymbol{p})}\right)^{1/2}, K^{(3,4)}_{2\uparrow}(\boldsymbol{p}) = -K^{(3,4)}_{2\downarrow}(\boldsymbol{p}) = \pm\frac{1}{2}(1-M/S)^{1/2}\left(\frac{\Sigma^*_{34}(\boldsymbol{p})}{2R_{34}(\boldsymbol{p})}\right)^{1/2}, \tag{7}$$

where the following notation has been used:

$$\Sigma_{12}(\boldsymbol{p}) = (M/S)c_z - \frac{1}{2}(c_x + c_y) + i\frac{\sqrt{3}}{2}(c_y - c_x),$$
$$\Sigma_{34}(\boldsymbol{p}) = -(M/S)c_z - \frac{1}{2}(c_x + c_y) + i\frac{\sqrt{3}}{2}(c_y - c_x).$$

III. CONDUCTIVITY AND MAGNETO-CONDUCTIVITY OF CANTED A-PHASE

It is straightforward to extend the standard "cross" technique for static defects[20] for the two-band model. As for the nature of the defects, when an ion B is substituted for an ion A in the unit formula $A_{1-x}B_xMnO_3$ it immediately lifts the cubic symmetry at the Mn-site. The e_g doublet gets split and the oxygen octahedron becomes distorted. Since, in accordance with our introductory remarks, this effect is of prime importance for the Mn-O-Mn conduction network, disorder in manganites to a large extent comes about through a change in doping. In application of diagrammatic cross-technique, however, we assume that positions of "impurities" (i.e. of B ions) remain random and there is no correlations between the scattering processes from any two of them. Secondly, for the "impurity" potential $U_{\alpha\beta}(\boldsymbol{r}-\boldsymbol{R_i})$ in

$$\widehat{H}_{imp}=\sum_i\int d^3\boldsymbol{r}\psi^\dagger_{\alpha\sigma}(\boldsymbol{r})U_{\alpha\beta}(\boldsymbol{r}-\boldsymbol{R_i})\psi_{\beta\sigma}(\boldsymbol{r}) \tag{8}$$

(where summation is held over the random realizations of the "impurities") one can assume the Jahn-Teller form of the defect potential. Using the basis given by Eq. (2), the expression for $U_{\alpha\beta}$ is:

$$U_{\alpha\beta}(\boldsymbol{r}-\boldsymbol{R_i})=gQ(\boldsymbol{R_i})\cdot\begin{pmatrix}0 & e^{i\theta_i}\\ e^{-i\theta_i} & 0\end{pmatrix}_{\alpha\beta}\cdot\delta(\boldsymbol{r}-\boldsymbol{R_i}), \tag{9}$$

where $Q(\boldsymbol{R_i})$ is an amplitude of the Jahn-Teller distortion at site i, g is an electron-lattice coupling constant and the angle θ_i specifies the shape of the distorted octahedron at a given Mn site. Going to momentum representation, the expression for $\widehat{H}_{imp}$ is:

$$\widehat{H}_{imp}=\sum_i\int\int\frac{d^3\boldsymbol{p}}{(2\pi)^3}\frac{d^3\boldsymbol{p'}}{(2\pi)^3}\widehat{a}^\dagger_{\alpha\sigma}(\boldsymbol{p})U_{\alpha\beta}(\boldsymbol{p}-\boldsymbol{p'})\widehat{a}_{\beta\sigma}(\boldsymbol{p'})\cdot e^{i(\boldsymbol{p}-\boldsymbol{p'})\cdot\boldsymbol{R_i}}, \tag{9a}$$

with

$$U_{\alpha\beta}(\boldsymbol{p})=\int d^3\boldsymbol{r}U_{\alpha\beta}(\boldsymbol{r})\cdot e^{-i\boldsymbol{p}\cdot\boldsymbol{r}}.$$

Keeping in mind the energy spectrum obtained in the preceding Section it is helpful to re-write expression (9a) in terms of new variables defined by (6):

$$\begin{aligned}\widehat{H}_{imp}=\sum_i gQ(\boldsymbol{R_i})\int\int\frac{d^3\boldsymbol{p}}{(2\pi)^3}\frac{d^3\boldsymbol{p'}}{(2\pi)^3}\sum_{l_1,l_2=1}^{4}\mathcal{M}^{(l_1l_2)}(\boldsymbol{p},\boldsymbol{p'};i)\cdot\widehat{\zeta}^\dagger_{l_1}(\boldsymbol{p})\cdot\ u(\boldsymbol{p}-\boldsymbol{p'})\cdot\ \widehat{\zeta}_{l_2}(\boldsymbol{p'})e^{i(\boldsymbol{p}-\boldsymbol{p'})\cdot\boldsymbol{R_i}},\\ \mathcal{M}^{(l_1l_2)}(\boldsymbol{p},\boldsymbol{p'};i)\equiv\sum_{\sigma=(\uparrow\downarrow)}\left\{K^{(l_1)*}_{1\sigma}(\boldsymbol{p})\cdot K^{(l_2)}_{2\sigma}(\boldsymbol{p'})\ e^{i\theta_i}+K^{(l_1)*}_{2\sigma}(\boldsymbol{p})\cdot K^{(l_2)}_{1\sigma}(\boldsymbol{p'})\ e^{-i\theta_i}\right\}.\end{aligned} \tag{9b}$$

The so-called "cross-technique"[20] can now be straightforwardly applied to the calculation of the average of new band Green function given by:

$$G_l(\boldsymbol{p},\boldsymbol{p'};t)=-i\langle\widehat{T}\left\{\widehat{\zeta}_l(\boldsymbol{p};0)\widehat{\zeta}^\dagger_l(\boldsymbol{p'};t)\right\}\rangle \tag{10}$$

In the absence of the defects, the Green function (10) is:

$$G^{(0)}_l(\boldsymbol{p};\varepsilon)=\frac{1}{\varepsilon-\xi_l(\boldsymbol{p})+i0\ \mathrm{sign}\varepsilon}, \tag{11}$$

where $\xi_l(\boldsymbol{p})=E_l(\boldsymbol{p})-E_F$ (again we can leave only four essential bands, since $J_H\gg|A|$). For the Green function averaged over defect's positions

$$\langle G(\boldsymbol{p},\boldsymbol{p'};\varepsilon)\rangle_{dis}=G(\boldsymbol{p};\varepsilon)\cdot\delta(\boldsymbol{p}-\boldsymbol{p'}) \tag{12}$$

we obtain the well known form of equation schematically shown in Fig.1. The self-energy part $\widehat{\Sigma}_l(\boldsymbol{p}-\boldsymbol{q};\varepsilon)$ on Fig.1 is again expressed in terms of the corresponding relaxation times as:

$$\widehat{\Sigma}_l(\varepsilon)=-i\ \mathrm{sign}\varepsilon\left\langle\frac{\hbar}{2\tau_l(\boldsymbol{p})}\right\rangle_{F.S.}, \tag{13}$$

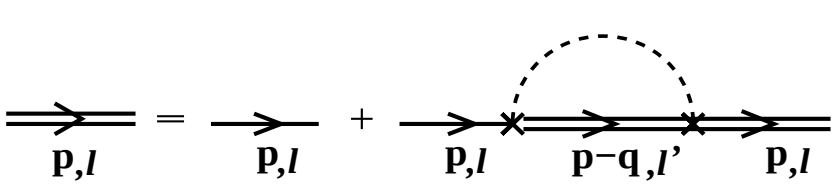

FIG. 1: Equation for an averaged over defects Green function (10). Summation over l' and integration over $\boldsymbol{q}$ are assumed.

where $\langle ... \rangle_{F.S.}$ denotes an average over the Fermi surface. Let us emphasize that attenuation τ_l in (13) contains contributions from scattering between different bands (5). In the representation (9b), the expressions for relaxation times $\hbar/2\tau_l$ are:

$$\frac{\hbar}{2\tau_l} = \pi \frac{|gQ|^2}{2\nu_l(E_F)} n_{imp} \int \frac{d^3\boldsymbol{p}}{(2\pi)^3} \int \frac{d^3\boldsymbol{p'}}{(2\pi)^3} \sum_{l_1=1}^{4} M^{(ll_1)}(\boldsymbol{p},\boldsymbol{p'}) \cdot \delta(E_F - E_{l_1}(\boldsymbol{p'})) \cdot M^{(l_1 l)}(\boldsymbol{p'},\boldsymbol{p}) \delta(E_F - E_l(\boldsymbol{p})),$$
$$M^{(l_1 l_2)}(\boldsymbol{p},\boldsymbol{p'}) \equiv \sum_{\sigma=(\uparrow,\downarrow)} \left\{ K_{1\sigma}^{(l_1)*}(\boldsymbol{p}) \cdot K_{2\sigma}^{(l_2)}(\boldsymbol{p'}) + K_{2\sigma}^{(l_1)*}(\boldsymbol{p}) \cdot K_{1\sigma}^{(l_2)}(\boldsymbol{p'}) \right\} \tag{14}$$

where n_{imp} is concentration of "impurities" (if our model with the potential (8-9) for Sr atom, one would have for $n_{imp} = x$, where x is a dopant concentration; we will come back to this in Section IV); $\nu_l(E_F)$ is a density of states at the Fermi level of the lth band. In the process of derivation of Eq. (14) we took into account that the main contribution to the integrals in Eq. (14) comes from the region close to the Fermi surface. We also used the following averages over disorder: $\langle (gQ(\boldsymbol{R}_i))^2 \rangle_{dis} = |gQ|^2$, $\langle e^{2i\theta_i} \rangle_{dis} = 1$ (the latter one means averaging over the local shapes of distorted octahedra).

With the use of Eqs. (13,14), the expression for the averaged Green function (12) can be written in the form:

$$\langle G_l(\boldsymbol{p},\boldsymbol{p'};\varepsilon) \rangle_{dis} = \delta(\boldsymbol{p}-\boldsymbol{p'}) \cdot \frac{1}{\varepsilon - \xi_l(\boldsymbol{p}) + i\,(\hbar/2\tau_l)\,\mathrm{sign}\varepsilon}. \tag{15}$$

The dc-conductivity can be calculated from the Kubo formula (see, for example, in [21]):

$$\sigma_{\alpha\alpha}(0) = \lim_{\omega \to 0} \frac{R_{\alpha\alpha}(\omega)}{i\omega}. \tag{16}$$

where $R_{\alpha\alpha}(\omega)(\alpha{=}x,y,z)$ can be obtained with the help of the corresponding product of retarded Green functions, averaged over impurities:

$$\langle R_{\alpha\alpha}(\omega) \rangle_{dis} = -\frac{ie^2\hbar}{(2\pi)} \int_{-\infty}^{\infty} d\varepsilon \sum_l \int \int \frac{d^3\boldsymbol{p}}{(2\pi)^3} \frac{d^3\boldsymbol{p'}}{(2\pi)^3} \left\langle \left(\widehat{\boldsymbol{v}}_\alpha^{(l)} \widehat{G}_l(\boldsymbol{p},\boldsymbol{p'};\varepsilon+\omega) \right) \cdot \left(\widehat{G}_l(\boldsymbol{p'},\boldsymbol{p};\varepsilon) \widehat{\boldsymbol{v}'}_\alpha^{(l)} \right) \right\rangle_{dis} \tag{17}$$

via analytic continuation $R_{\alpha\alpha}(i\omega_n) \to R_{\alpha\alpha}(\omega + i\delta)$ (in Eq. (17) $\widehat{\boldsymbol{v}}_\alpha^{(l)}$ is the velocity operator defined as a derivative of energy with respect to the momentum for each band given by Eqs. (5)). With the impurity potential given by Eqs. (9, 9a), the average of product in expression (17) can be re-written as

$$\left\langle \widehat{\boldsymbol{v}}_\alpha^{(l)} \widehat{G}_l(\boldsymbol{p},\boldsymbol{p'};\varepsilon+\omega) \cdot \widehat{G}_l(\boldsymbol{p'},\boldsymbol{p};\varepsilon) \widehat{\boldsymbol{v}'}_\alpha^{(l)} \right\rangle_{dis} = \widehat{\boldsymbol{v}}_\alpha^{(l)} \left\langle \widehat{G}_l(\boldsymbol{p},\boldsymbol{p'};\varepsilon+\omega) \right\rangle_{dis} \cdot \left\langle \widehat{G}_l(\boldsymbol{p'},\boldsymbol{p};\varepsilon) \right\rangle_{dis} \widehat{\boldsymbol{v}'}_\alpha^{(l)}. \tag{18}$$

Now, taking into account equations (12-18) and performing the integration in (17) with respect to ε, we finally obtain the following expression for the in-plane and out-of-plane dc-conductivities:

$$\begin{aligned} \sigma_{xx} &= \sigma_{xx}^{(+)} + \sigma_{xx}^{(-)}, \\ \sigma_{zz} &= \sigma_{zz}^{(+)} + \sigma_{zz}^{(-)}, \end{aligned}$$

where

$$\begin{aligned} \sigma_{\alpha\alpha}^{(+)} &= (1 + M/S)^2 \cdot \frac{e^2}{a\hbar} \int_{F.S.} \sum_{l=1}^{2} \frac{\tau_l}{\hbar} \cdot \frac{dS_{\boldsymbol{p}}^l}{|\nabla_{\boldsymbol{p}} E_l|} \left(\frac{\partial E_l(\boldsymbol{p})}{\partial \boldsymbol{p}_\alpha} \right)^2, \\ \sigma_{\alpha\alpha}^{(-)} &= (1 - M/S)^2 \cdot \frac{e^2}{a\hbar} \int_{F.S.} \sum_{l=3}^{4} \frac{\tau_l}{\hbar} \cdot \frac{dS_{\boldsymbol{p}}^l}{|\nabla_{\boldsymbol{p}} E_l|} \left(\frac{\partial E_l(\boldsymbol{p})}{\partial \boldsymbol{p}_\alpha} \right)^2, \end{aligned} \tag{19}$$

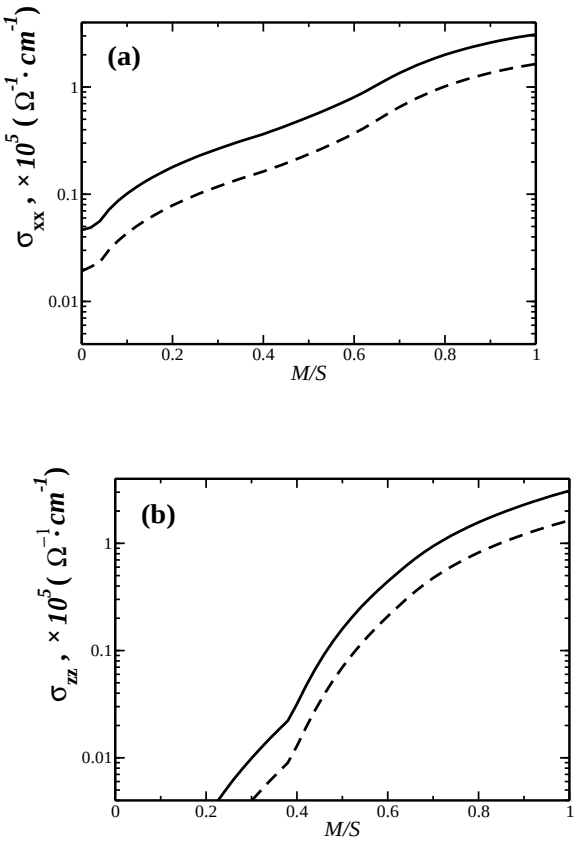

FIG. 2: In-plane (a) and out-of-plane (b) conductivities in the canted A-phase are shown on log scale as a function of M/S for different values of $\Delta = |gQ|/|A|$. Solid (dashed) lines correspond to the $\Delta = 0.45$ (0.75). Both curves are obtained for dopant concentration $x = 0.55$ and $a = 3.9\mathring{A}$. The dependence $E_F(M/S)$ is presented below on Fig.3.

where $\hbar/\tau_l (l = 1, 2, 3, 4)$ are defined by Eq. (14), $\alpha = (x, z)$ and integration runs over each Fermi surface.

Expressions (19) for both in-plane and out-of-plane conductivities are rather complicated and the procedure of evaluating the conductivity using them deserves further explanation. Parameters of the electronic spectrum are chosen beginning with the initial two-band "cubic" phase which, as we believe, realizes itself in the ferromagnetic state. Let us also recall that the disorder in the calculations presented above expresses itself through the local octahedra distortion which, in turn, is produced by the substitutional disorder, i.e. by non-stoichiometric $A_{1-x}B_xMnO_3$. Therefore, in (19) the "concentration" of "impurities" is the concentration of B atoms, while the amplitude of the disorder potential is given by the value of $|gQ|$ in Eq. (14). Change in composition by increasing x decreases the number of carriers, $1 - x$, while increasing the number of defects *simultaneously*. Another significant simplification above was that the distortions of the oxygen octahedra were treated independently. Indeed this is a good approximation, because two octahedra surrounding two neighboring Mn atoms share one oxygen atom only. If it were not so, the values of resistivity would depend on the B atom concentration only. In reality a sample's quality also depends on how these octahedra adjust themselves. Factor n_{imp} in (14) is not the only reason for dependence of conductivity on x in (19). Change in carrier concentration results in a shift of the chemical potential relative to the bottom of the bands which reflects itself in an immediate change in the occupation number in each of the four active energy bands (5). Such a non-trivial intimate dependence between the number of carriers and the number of defects presents itself as a new feature for conductivity behavior in manganites. It would be of great interest to investigate such a trend experimentally. Currently a shortage of experimental data for LSMO compounds for large enough Sr concentrations deprives us the possibility to trace that dependence in some more details. Some estimates have been done for the FM-phase in our previous paper[12] for $x = 0.3 \div 0.4$. In this presentation we perform the calculations for canted A-phase for $x = 0.55$. In Fig. 2(a,b) we plotted our results. Energy spectrum of the A-phase itself in the DE approximation ($J_H \gg |A|$) would not allow current to flow in the out-of-plane direction: the dispersion $t(p_z) \propto \cos(p_z)$ drops out from (5) for $M = 0$. Therefore Fig. 2 describes, as expected, a dramatic magneto-resistance effect inherent to the

canted A-phase for the perpendicular-to-the-plane current (σ_{zz}). Surprisingly, it turned out that even the in-plane (σ_{xx}) components of conductivity display considerable change in its value at the transition from the 3D conductivity regime in the ferromagnetic state (i.e. at $M/S = 1$) to the 2D one for the A-phase ($M = 0$). The origin of such a rapid change comes about from the re-distribution of carriers between the energy bands with change in the value of M/S. The effect of carrier re-distribution in the bands is seen in Fig. 3 which shows the calculated position of the Fermi level for doping concentration $x = 0.55$. With variation of M/S the system undergoes dimensional transition between the 2D and 3D conductivity regimes.

In Fig. 2 (a,b) it seemed more convenient to present our results for the chosen concentration as a function of M/S in accordance with Eqs. (18). We remind that M is a ferromagnetic component of the *core spins* only. In order to find the values of conductivity as a function of the total magnetization, $\widetilde{M}$, which also includes the electronic component and is induced by an external magnetic field, one may use the following simple relation:

$$\widetilde{M} = \mu_B(4 - x) \cdot (M/S). \tag{20}$$

Equation (20) expresses the value of the full magnetic moment $\widetilde{M} = \chi B$, in units of Bohr magneton per Mn ion, and χ is a magnetic susceptibility.

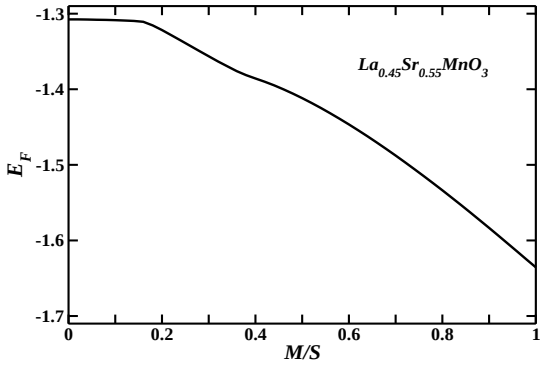

FIG. 3: The dependence of E_F on M/S for a given concentration $x = 0.55$ based on band structure described by (5). E_F is given in the units of the hopping amplitude $|A|$ (see Eq. (5)). The reference point for the Fermi level is taken at the bottom of the lowest band.

IV. CHARGES AND SPINS NEAR INTERFACE

We now turn to some problems which involve artificial contacts of manganites with different magnetic ground states or just two manganites having the same ground states but different doping concentrations. We will discuss both charge and magnetic structure in the vicinity of the boundary. Below we consider the plane geometry, so that all quantities depend on one coordinate only. In addition we simplify our discussion by choosing the single band DE model $T^{\alpha\beta} \to t$, where t is a hopping amplitude.

We first consider two ferromagnetic manganites with different doping concentrations brought into contact with each other with the parallel orientations of the local moments. Some pronounced effects come about due to the Schottky layers formed at the contact. Difference in doping concentrations produces a difference in the chemical potentials on both sides away from the contact, ${E_F}^{left}$ and ${E_F}^{right}$, i.e. difference in the "work functions" of two components. That leads to a redistribution of carriers near the contact plane. This effect is general and well known for the contacts between metals or semiconductors. A simplifying feature for the contacts of two manganites is in similarity of the underlying band structures on the both sides of a contact. At the same time all major changes still take place at the atomic scale so that one needs to apply the Kohn-Sham scheme to solve for potential and charge distributions self-consistently. To elucidate some qualitative features we provide in Appendix the solution of this problem in its continuous formulation.

We proceed as follows. Let $N_{L(R)}$ be the concentration (i.e. the number per cm^2) of positive charges in (LaSr) plane on the left(right) side far away from the contact. In the process of preparation of the hetero-structure (film

deposition)[5], the Sr concentration N_{Sr} changes sharply from N_L to N_R at the contact. The system of Kohn-Sham equations (the Poisson equation for the potential distribution and the Schrödinger equation) is:

$$\begin{aligned} \Phi(i+1) - 2\Phi(i) + \Phi(i-1) = \frac{4\pi e^2}{t}\left[N_{Sr}(i) - n_{el}(i)\right], \\ -\Psi_\lambda(i+1) + 2\Psi_\lambda(i) - \Psi_\lambda(i-1) + \Phi(i)\Psi_\lambda(i) = E_\lambda \Psi_\lambda(i), \end{aligned} \tag{21}$$

where i is an index, which runs through the Mn planes, λ is an eigenvalue index, E_λ is an energy in units of t, Φ is a dimensionless potential defined by electrostatic potential $\varphi(i)$ as

$$\Phi(i) = -\frac{|e|\varphi(i)}{t}, \tag{22}$$

$n_{el}(i) = \sum_{\lambda<\lambda_F} |\Psi_\lambda(i)|^2$ is a concentration of electrons on a plane i and $N_{Sr}(i)$ is a Sr concentration, which depends on which side of the contact an electron is located and $E_{\lambda_F} = E_F(i)$ with $E_F(i)$ being equal to the local Fermi level in the units of t. We have obtained a numerical solution of (21) with the boundary conditions providing the equality of the electrochemical potentials across the contact. In the calculations below the total number of layers was equal to twenty (ten on each side of the contact) with:

$$N_{Sr}(i) = \begin{cases} 0.6, & i \le 10, \\ 0.4, & i > 11. \end{cases} \tag{23}$$

The solution for the potential and electron distribution is shown on Fig. 4(a,b). The consistency of our numerical results have been verified by comparing them with the analytical ones obtained from the solution of the same problem in its continuous form. The latter are described in Appendix in more details.

The significance of these calculations for the further discussion is as follows. First of all, one sees that the electron screening (the "Thomas-Fermi" length) extends over four-five atomic distances implying that the sharpness of the contact is smoothed out considerably. Secondly, there is a re-distribution of charge between phases: repletion and depletion regions form close to the interface.

We now turn to the discussion of a contact between the manganites in the ferromagnetic and anti-ferromagnetic A-phase. The results of the previous Section have demonstrated the pronounced magneto-resistance effects in the canted A-phase for both in-plane and out-of-plane directions of a current. This justifies an interest and need for better understanding of the F/A contact properties.

Stacks of manganite films of different thickness with abrupt change in Sr concentration in the (LaSr) planes in order to stabilize FM- or A-phase, can be made using the state of the art deposition techniques[5]. However contacts between the FM state and the A-phase studied in[5] pose more questions than the preceding example of the contact between the two unequally doped ferromagnetic metallic manganites. Schematically such a contact is shown on Fig. 5 in the plane geometry. A transitional layer lies in the shaded area and its structure may become complicated by a number of reasons. First of all one should expect that the charge effects discussed above for a contact between the two FM phases exists at present case as well. Re-distribution of the carriers may shift the boundary between the magnetic phases. Less clear is the magnetic structure of such a transitional layer: whether there is a sharp boundary for the spins orientations on both sides of a contact or the direction of spins may rotate going through the interface from left to right, needs further discussion. In particular, since the energy of magnetic anisotropy in manganites is rather weak (magnetization of ferromagnetic manganites is saturated[22] at external fields of the order of 100 Oe) orientation of moments in Fig. 5 may even change gradually forming a structure similar to the one in the Bloch or Neel domain wall. The transitional region between the two phases may include a canted A-phase, magneto-conductivity of which has been studied above. It is highly desirable to further address these issues experimentally.

V. DISCUSSION AND SUMMARY

We return to the applicability of our band model for different doped manganites. Preparation of high-quality samples needs significant efforts and therefore experiments with doped manganites having good metallic conductivity at low temperatures are rare in the literature. Ferromagnetic metallic LSMO samples [5,16] with $\rho_0 \simeq 10^{-5}\ \Omega \cdot cm$ have been reported. Estimates of Ref. [12] give mean free path values as large as $l \simeq 80a$. More typical values of residual resistivity are of the order of 1 $m\Omega \cdot cm$[12], which means that the mean free path lies on the scale of several inter-atomic distances. Higher values of resistivity often correlate with larger mismatch in the ionic radii of the constituent elements (tolerance factor $t < 1$).

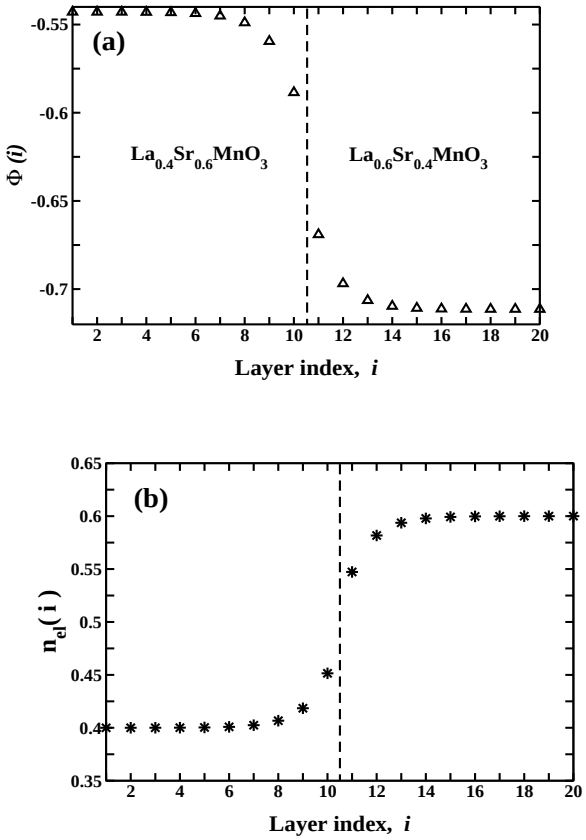

FIG. 4: Contact of two metallic ferromagnetic phases with different Sr concentrations in the one band DE model. The numerical solution of Kohn-Sham equations is shown for the structure with number of layers being equal to twenty. The dashed line shows the position of the (La,Sr) plane, where the abrupt change in Sr concentrations takes place; a) Potential $\Phi(i)$ is given in dimensionless units $4\pi e^2/(at)$; b) $n_{el}(i)$ is concentration of electrons in the layer i in units of a^{-2}, where a is a lattice constant.

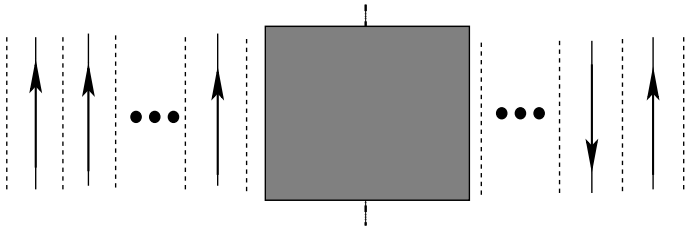

FIG. 5: Schematic presentation of a contact between ferromagnetic (left) and A-phase (right) manganites. Shaded area designates the interface region. The dashed lines designate the (LaSr) layers (the long dashed line in the middle singles out the plane (interface layer) in which the Sr concentration is sharply changed). Full lines designate the MnO planes in which carriers are positioned. The directions of the arrows in Fig. 5 to the left and to the right from the interface show the magnetic order in the FM- and A-phase correspondingly.

From various experimental data on A-phase in manganites $Pr_{0.5}Sr_{0.5}MnO_3$, $Nd_{0.45}Sr_{0.55}MnO_3$ and $La_{0.45}Sr_{0.55}MnO_3$ [4,5] the values of the in-plane resistivity of these compounds lie in the range $\rho \sim 3 \div 7$ ($m\Omega{\cdot}cm$). In these samples one obviously has the conductivity regime in the A-phase lying close to the mobility edge. As we have seen, magnetoconductivity and other properties of the A-phase are interesting enough to justify the efforts to improve the values of resistivity in the A-phase manganites. As for the LSMO films and hetero-structures prepared in[5], the value of residual resistivity in the ferromagnetic state of $La_{0.6}Sr_{0.4}MnO_3$ compound and the value of the in-plane residual resistivity of the A-phase $La_{0.45}Sr_{0.55}MnO_3$ compound are $\rho_0 = 8 \cdot 10^{-4}\ \Omega \cdot cm$ and $\rho_0 = 3 \cdot 10^{-3}\ \Omega \cdot cm$ re-

spectively. The films were prepared by a pulsed deposition method and obviously are not clean enough. Nevertheless, qualitatively there is an agreement: our calculations of the values of resistivity for ferromagnetic phase and A-phase (when $M = 0$) for the Sr concentrations $x = 0.4$ and $x = 0.5$ correspondingly gave a factor of ten difference while the experimentally observed difference is only a factor of two.

As far as an interface is concerned, the complications that lie on the theory part are as follows. The DE mechanism that played such an important role in exploring the properties of the half-metallic magnetic ground state, bears a non-local character. Therefore it is not straightforward to account for it in an inhomogeneous problem with a spatial dependence near the interface (recently, there were attempts to present the DE mechanism in a local form to describe the various domain structures in FM metallic manganites[3]). Secondly, diminishing the number of band electrons, the anti-ferromagnetic super-exchange interaction between the t_{2g} spins becomes comparable with the DE interaction. The task of combining these two mechanisms to study an inhomogeneous problem is already a serious problem.

The A-phase ground state has been found in a number of other compounds, such as $Pr_{0.5}Sr_{0.5}MnO_3$ and $Nd_{0.45}Sr_{0.55}MnO_3$[2,23]. The transition into the A-phase along the temperature axis is of the first order as it is expected from symmetry considerations. It is accompanied by a change in the c/a ratio[5,7]. Such a transition is often described in the literature in terms of the "orbital ordering"[15]. We suggest to interpret this transition as a cooperative Jahn-Teller effect involving the proper lattice distortion. Indeed, so far we have discussed changes in the electronic band structure caused by spin re-arrangements only. Meanwhile, as it was discussed in Introduction, lattice effects may also play an important role. Judging from various experimental results (for a review, see[4]), the importance of the lattice effects may vary and depend on a specific compound. For example, the lattice deformations strongly prevail in $Nd_{0.45}Sr_{0.55}MnO_3$ compound[2]. Its ground state shows huge anisotropy in resistivity ($\rho_c/\rho_{ab} \sim 10^4$) and much lower in-plane conductivity compared to other members of the A-phase family[5,23]. As it was shown in Ref. [12] the strong enough shear deformation $d_{x^2-y^2}$ of the oxygen octahedra ($c/a < 1$) alone may lead to a in practically two-dimensional electronic spectrum. We suppose that $Nd_{0.45}Sr_{0.55}MnO_3$ is such an extreme case ($t \simeq 0.95$)[4]. After carriers are added to the 2D bands both their and core spins adjust themselves via DE and super-exchange mechanisms. If in other A-phase compounds the tetragonal deformations of the lattice, $c/a < 1$, is less pronounced, one may neglect it as we have done above for $La_{0.45}Sr_{0.55}MnO_3$. The phase diagram for the $La_{1-x}Sr_xMnO_3$ as a function of Sr doping x and fixed tetragonal distortion c/a has been theoretically studied in[24]. We note, that the Jahn-Teller interaction has not been considered in[24] and the electronic band structure was obtained for a fixed values of c/a.

Much attention in Ref. [5] was also given to the characterization of properties of the hetero-structures consisting of mixed phases [F_n, A_m] (n and m are the number of unit cells per period of the structure). Major conclusion drawn by the authors[5] from data on magnetization, structural characterization of the modulated films and their in-plane conductivity have led them to the notion of stable FM and A-phase single layers, which preserve their integrity and stability even in very thin intervening structures such as $n, m = 2 \div 5$. This result supports the point that stability of the A-phase layers is due to the coherent octahedra shrinkage, $c/a < 1$, in the planes. Such an idea leaves room for speculation regarding the possible spin arrangements in the heterostructures.

It is interesting that the conductivity measurements for the samples with composition [F_{10}, A_{10}] gave lower values of conductivity as if it were due to the FM layers alone. We ascribe this to the effect of charge re-distribution shown in Fig. 4(b): ferromagnetic layers having more carriers supply part of them to the A-phase layers. Ten layers of each phase is already a good approximation for the picture of a single interface, as it is seen in Fig. 5. With n and m decreased, the role of Coulomb effects becomes weaker and each layer preserves its nominal composition and, hence, the in-plane conductivity.

One more comment we would like to add to the latter point concerns a pronounced increase in magneto-conductivity toward the [F_3, A_3] samples. If the number of electrons on each FM- and A-phase planes does not change, the positive magneto-conductivity effect is an indication of stronger canting of the moments in these samples. (Recall that large values of in-plane magneto-conductivity on Fig. 2(a) is a result of changing Fermi level at the transition between the 2D and 3D regimes). Data provided by[5] qualitatively agree with our results for the values of in-plane conductivity for the canted A-phase (Fig. 2(a)).

To summarize, we have determined the electronic spectrum for the canted A-phase and calculated both conductivity and magneto-conductivity of such a ground state. Calculations have been done in the framework of the two-band model[12]. Disorder introduced by the substitutional doping results in an intimate correlation between conductivity and number of carriers. Defects are described in terms of random Jahn-Teller centers. Magneto-resistivity for both in-plane and out-of-plane directions are expressed in terms of magnetization, the latter can be measured independently. Negative in-plane magneto-resistivity turns out to be large. Our study of effects at the contact between the two phases showed rather large screening length of the order of five unit cells. We suggest that in the transition to the A-phase the Jahn-Teller cooperative ordering plays a leading role. The resulting magnetic structure determines the final electronic band spectrum. We applied the results of the present paper to discuss the data obtained in[5]. There is a qualitative agreement of experimental data with our results and conclusions above. More experimental work is needed to further investigate interesting properties of the A-phase and heterostructures in the presence of an external

magnetic field.

VI. ACKNOWLEDGMENTS

This work (M.D. and L.P.G.) was supported by the NHMFL through the NSF cooperative agreement DMR-9527035 and the State of Florida and by DARPA through the Naval Research Laboratory Grant No. N00173-00-1-6005. The work of (V.Z.K.) was supported by DARPA under Contract No. 01J543.

APPENDIX A: SOLUTION OF THE POISSON EQUATION FOR THE INTERFACE IN THE CONTINUOUS MODEL.

Here we will present the exact solution of the Eq. (21) in the continuous limit. In that case, we can solve the Poisson equation on each side of the contact will and, after using the boundary conditions are able to obtain a general solution.

If the plane of the interface coincides with yz plane, the potential will depend on x only. We assume the spectrum of the electrons to have a parabolic form: $\varepsilon(k) = k^2/2m$. The concentration of electrons is given by:

$$n_{el}(x) = \frac{(2m)^{3/2}}{3\pi^2\hbar^3}\left[\mu(x)\right]^{3/2}, \tag{A1}$$

where $\mu(x)$ is a local chemical potential. Taking into account (A1), we have to solve the Poisson equation:

$$\frac{d^2\Phi}{dx^2} = \frac{4\pi e^2}{t}\left[N_{Sr}(x) - n_{el}(x)\right], \tag{A2}$$

where N_{Sr} is a Sr concentrations defined by:

$$N_{Sr}(x) = \begin{cases} N_L, & x \le 0, \\ N_R, & x \ge 0, \end{cases} \tag{A3}$$

We introduce the following notations: $\mu(x) + \Phi(x) = \zeta = const$, where ζ is an elechtro-chemical potential and $\Phi(x)$ is:

$$\Phi(x) = \begin{cases} \Phi_L(x), & x \le 0, \\ \Phi_R(x), & x \ge 0, \end{cases} \tag{A4}$$

The boundary conditions for the potential preserving the charge conservation are:

$$\Phi_L(0) = \Phi_R(0), \ \frac{d\Phi_L}{dx} = \ \frac{d\Phi_R}{dx}|_{x=0}. \tag{A5}$$

Introducing $V(x) = \zeta - \Phi(x) > 0$ and using (A1) and (A5), Eq. (A2) is re-written as:

$$\frac{d^2V(x)}{dx^2} = \frac{4\pi e^2(2m)^{3/2}}{3\pi^2\hbar^3}\cdot\left\{V^{3/2}(x) - V^{3/2}(\pm\infty)\right\}, \tag{A6}$$

where

$$\frac{4\pi e^2(2m)^{3/2}}{3\pi^2\hbar^3}\cdot V^{3/2}(\pm\infty) = N_{\pm}.$$

The first integral of Eq. (A6) has the following form:

$$\left(\frac{dv}{dx}\right) = \frac{1}{\kappa^2}\left[\frac{2}{5}v^{5/2}(x) - v(x) + \frac{3}{5}\right], \qquad v(x) = V(x)/V(\pm\infty), \tag{A7}$$

where $\kappa^2 \equiv (3\pi\hbar^3)/(8e^2(2m)^{3/2})$. Equation (A7) can be presented as:

$$\frac{dv}{\sqrt{(2/5)v^{5/2} - v + (3/5)}} = \pm\sqrt{2}\kappa dx, \tag{A8}$$

where plus(minus) sign corresponds to $v_{L(R)}(x)$. Integral on the left hand side of Eq. (A8) can be calculated exactly. The final result reads:

$$\begin{aligned}\Phi\left[V(x)\right] &= \pm\frac{\kappa x}{\sqrt{10}}+C,\\ \Phi\left[V(x)\right] &= \sqrt{a_1-a_2x}\cdot\left\{2\sqrt{a^*{}_1-a^*{}_2x}\cdot(x+\alpha)\cdot F[\phi_1,m_1]-\right.\\ &\left. b_1\cdot\sqrt{a_2\cdot(x+\alpha)^2\cdot(b_2+b_3\cdot x)}\cdot\Pi[n_1;\phi_2,m_2]\right\}/\left\{\sqrt{(x+\alpha)\cdot(x^2+|\beta|^2)}\right\},\end{aligned} \tag{A9}$$

where F and Π are elliptic integrals of the first and third kind correspondingly and $\{a_i, b_i, \phi_i, m_i\}$ are complex numbers. Making use of boundary conditions (A5) recovers the results obtained numerically on Fig.4(a,b).

It is also useful to obtain the solution of the Poisson equation (A2) in the linear approximation, assuming $\Phi(x)$ is small compared to ζ. After very simple algebra, (A2) takes the following form:

$$\frac{d^2\Phi(x)}{dx^2}=\frac{1}{\lambda^2}\left[\Phi(x)-\Phi(\pm)\right], \tag{A10}$$

where

$$\begin{aligned}\frac{1}{\lambda^2}&=\left(\frac{2e^2(2m)^{3/2}}{\pi\hbar^3}\right)\cdot\zeta^{1/2},\\ \Phi(\pm\infty)&=\frac{(2m)^{3/2}/(3\pi^2\hbar^3)\cdot\zeta^{3/2}-N_{L(R)}}{2(2m)^{3/2}/(2\pi^2\hbar^3)\cdot\zeta^{1/2}}.\end{aligned} \tag{A11}$$

Taking into account the boundary conditions (A5), the integration of (A11) is straightforward. Thus the solution of (A11) reads:

$$\Phi(x)=\begin{cases}\Phi(+\infty)+\delta\Phi\cdot e^{-x/\lambda}, & x\geq 0,\\ \Phi(-\infty)-\delta\Phi\cdot e^{x/\lambda}, & x<0,\end{cases} \tag{A12}$$

where the notation $\delta\Phi=0.5\cdot(\Phi(-\infty)-\Phi(+\infty))$ was introduced for brevity. As it is easy to see, the result given by (A12) reproduces all the features of our numerical solution shown in Fig. 4(a,b).

[1] S. S. P. Parkin, Annu. Rev. Mater. Sci. **25**, 357 (1995).
[2] H. Kuwahara, T. Okuda, Y. Tomioka, A. Asamitsu and Y. Tokura, Phys. Rev. Lett. **82**, 4316 (1999).
[3] see D. I. Golosov, *pre-print* **cond-mat/0206257** and references there in.
[4] Y. Tokura and Y. Tomioka, Jour. of. Magn. and Magn. Mat. **200**, 1 (1999).
[5] M. Izumi, T. Manako, Y. Konishi, M. Kawasaki, and Y. Tokura, Phys. Rev. B **61**, 12187 (2000).
[6] H. Tanaka, J. Zhang and T. Kawai, Phys. Rev. Lett. **88**, 027204 (2002).
[7] Y. Tokura, A. Urushibara, Y. Moritomo, T. Arima, A. Asamitsu, G. Gido and N. Furukawa, J. Phys. Soc. Jpn. **63**, 3931 (1994).
[8] A. Urushibara, Y. Moritomo, T. Arima, A. Asamitsu, G. Kido and Y. Tokura, Phys. Rev. B **51**, 14103 (1995).
[9] H. Fujishiro, M. Ikebe, and Y. Kohno, J. Phys. Soc. Jpn. **67**, 1799 (1998).
[10] C. Zener, Phys. Rev. **82**, 403 (1951); P. W. Andreson, H. Hasegawa, Phys. Rev. **100**, 675 (1955).
[11] E. Dagotto, T. Hotta and A. Moreo, Physics Reports **344**, 1 (2001).
[12] L. P. Gor'kov and V. Z. Kresin, JETP Lett. **67**, 985 (1998); M. Dzero, L. P. Gor'kov and V. Z. Kresin, Eur. Phys. Jour. **B**, 459 (2000).
[13] J. van der Brink and D. Khomskii, Phys. Rev. Lett. **82**, 1016 (1999).
[14] I. V. Solovyev and K. Terakura, Phys. Rev. Lett. **83**, 2825 (1999); I. V. Solovyev, Phys. Rev. **63**, 174406 (2001).
[15] K. I. Kugel, D. I. Khomskii, Sov. Phys. JETP **37**, 725 (1973).
[16] M. Quijada, J. Cerne, J. R. Simpson, H. D. Drew, K. H. Ahn, A. J. Millis, R. Shreekala, R. Ramesh, M. Rajeswari and T. Venkatesan, Phys. Rev. B **58**, 16093 (1998).
[17] Y. Konishi, Z. Fang, M. Izumi, T. Manako, M. Kasai, H. Kuwahara, M. Kawasaki, K. Terakura, and Y. Tokura, J. Phys. Soc. Jpn. **68**, 3790 (1999).
[18] Y. Moritomo, T. Akimoto, H. Fujishiro, A. Nakamura, Phys. Rev. B **64**, 064404 (2001).
[19] P.-G. de Gennes, Phys. Rev. **118**, 141 (1960).
[20] A. A. Abrikosov, L. P. Gorkov and I. E. Dzyaloshinski, *Methods of Quantum Field Theory in Statistical Physics* (Dover Publications, New York, 1975).

[21] S. Doniach and E. H. Sondheimer, *Green's functions for solid state physics* (Imperial College Press, London, 1999).
[22] J. M. D. Coey, M. Viret and S. von Molnar, Adv. Phys. **48**, 167 (1999).
[23] Y. Tomioka, A. Asamitsu, Y. Moritomo, H. Kuwahara and Y. Tokura, Phys. Rev. Lett. **74**, 5108 (1995).
[24] Z. Fang, I. V. Solovyev and K. Terakura, Phys. Rev. Lett. **84**, 3169 (2000).